Engineered Lipid Bicelle Nanostructures for Membrane-Disruptive Antibacterial Applications

Tun Naw Sut[a,b,1], Elba R. Valle-González[a,1], Bo Kyeong Yoon[b,1], Soohyun Park[a], Joshua A. Jackman[*,b], Nam-Joon Cho[*,a]

[a]School of Materials Science and Engineering, Nanyang Technological University, 50 Nanyang Avenue 639798, Singapore
[b]School of Chemical Engineering and Biomedical Institute for Convergence at SKKU (BICS), Sungkyunkwan University, Suwon 16419, Republic of Korea

[1]These authors contributed equally to this work.

*E-mail address: njcho@ntu.edu.sg and jjackman@skku.edu

Abstract

Lipid bicelles are cell membrane-mimicking nanostructures that self-assemble from mixtures of long- and short-chain lipidic components and are widely used in various applications related to structural biology, drug delivery, and interfacial science. To date, most research efforts have focused on bicelles as passive structural carriers to host membrane proteins or hydrophobic drugs, while there remains untapped potential to engineer functionally active lipid bicelles that contain biologically important lipidic components for targeted applications. Herein, we developed antibiotic-free, antibacterial bicellar nanostructures composed of a long-chain phospholipid and glycerol monolaurate, which is a monoglyceride that exhibits membrane-disruptive inhibitory activity against various bacteria and membrane-enveloped viruses. Quartz crystal microbalance-dissipation and time-lapse fluorescence microscopy imaging experiments were conducted to identify fusogenic bicellar compositions with optimal levels of pore-like, membrane-disruptive activity that was distinct from the activity of the monoglyceride alone. Cryogenic transmission electron microscopy was performed to characterize the lamellar-phase nanostructure properties of the lead bicelle composition along with *in vitro* antibacterial assays, which identified that the bicelles inhibited *Staphylococcus aureus* bacteria *via* a killing mechanism. Collectively, these findings demonstrate the potential of applying molecular-level engineering strategies to fabricate lipid bicelles with membrane-disruptive properties relevant to anti-infective applications.

Keywords: bicelle; self-assembly; nanostructure; membrane disruption; antibacterial

1. Introduction

Lipid bicelles, which are also known as bilayered mixed micelles and lipid nanodiscs, are cell membrane-mimicking nanostructures that self-assemble from long- and short-chain lipidic components [1-3]. Bicelles are conventionally viewed as quasi-two-dimensional disks that form due to long-chain lipid components self-assembling into a planar bilayer while short-chain lipid components form a rim around the bilayer edges [4]. The experimentally observed morphologies of bicelles are more varied and also include other types of nanostructures such as worm-shaped micelles, perforated lamellar sheets, and vesicle-shaped aggregates [5-11]. The precise morphology of a bicellar system depends on numerous factors such as the total lipid concentration, molar ratio of long- to short-chain lipidic components ("q-ratio"), lipid composition, and temperature. The ability to rationally tune these design parameters highlights how bicelles can be viewed within the nanoarchitectonics concept as functional supramolecular assemblies built from nanoscale molecular components [12,13].

To date, the major scope of bicelle applications has been in the structural biology field, where they provide a membrane-mimetic environment to host membrane proteins for structural and functional investigations [14-16]. Bicelles have also been used as carriers in drug delivery applications and can encapsulate hydrophobic drugs to enhance solubility and cellular uptake [17-19]. One of the most active application areas is transdermal drug delivery because lipid bicelles have suitable structural properties to pass through the outer layer of skin [20-24]. The encapsulation of a wide range of biologically active pharmaceutical drugs and cosmetic agents in bicelles has been explored for skincare applications [25-28]. In these past studies, bicelles have been mainly viewed as nanostructured carriers while recent findings in the material science field demonstrate that bicelles are also useful functional tools to fabricate supported lipid bilayers [29-38]. Importantly, such fabrication capabilities have been reported with lipid bicelles containing natural molecular components [39-41], leaving open the door to further explore whether biologically active natural components can be functionally incorporated into bicellar nanostructures as part of application-directed bicelle engineering strategies. Such efforts fit within broader trends in the field to develop various classes of organic and inorganic nanoparticles with functional capabilities to inhibit microbial pathogens such as bacteria and viruses [42-45].

Towards this goal, herein, we investigated the development of antibacterial bicellar nanostructures composed of long-chain 1,2-dioleoyl-*sn*-glycero-3-phosphocholine (DOPC) lipid and glycerol monolaurate (GML), which is a monoglyceride that has a twelve-carbon long, saturated hydrocarbon chain and exhibits membrane-disruptive activity against a wide range of pathogens such as bacteria and membrane-enveloped viruses [46-50]. Nanoscale, oil-in-water GML emulsions have been reported to exhibit antibacterial activity [51,52], while dilution-stable, fully aqueous nanostructured assemblies have not been reported and it is also unknown whether GML retains membrane-disruptive activity when incorporated into lipid nanostructures. **Fig. 1** outlines the experimental scope to fabricate and evaluate the structural and membrane-disruptive properties of DOPC-GML bicelles in biophysical and biological application contexts. Our integrated approach across biophysical and biological experiments enabled us to identify lamellar-phase DOPC-GML bicelle compositions that exhibited pore-like, membrane disruption along with antibacterial activity *via* a killing mechanism. Since GML is known to be mainly active against Gram-positive bacteria rather than Gram-negative bacteria [47], we selected *Staphylococcus aureus* (*S. aureus*) as a model Gram-positive bacterium for antibacterial testing and it is a leading cause of bacterial infections as well as a major public health threat, especially with the rise of antibiotic-resistant strains [53].

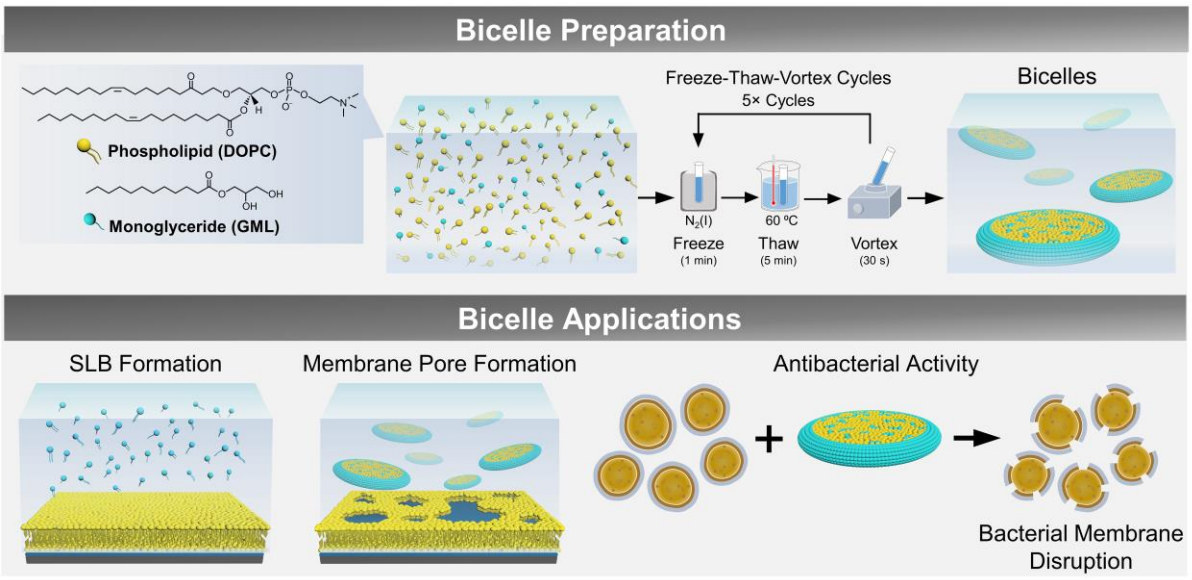

Fig. 1. Experimental strategy to develop membrane-disruptive lipid bicelles for anti-infective applications. Bicelles were prepared by the hydration of lipid mixtures followed by freeze-thaw-vortex processing. The adsorption, fusogenic, and membrane-disruptive properties of bicelle candidates were evaluated along with structural characterization and antibacterial testing of the lead bicelle composition.

2. Materials and methods

2.1. Bicelle preparation

Bicelles composed of DOPC phospholipid (Avanti Polar Lipids, Alabaster, AL) and GML (Abcam, Cambridge, UK) or 1,2-dihexanoyl-*sn*-glycero-3-phosphocholine (DHPC; Avanti Polar Lipids) were prepared at the specified q-ratio, as previously described [39-41]. For fluorescence microscopy measurements, a 99.5:0.5 molar ratio of DOPC and 1,2-dioleoyl-*sn*-glycero-3-phosphoethanolamine-N-(lissamine rhodamine B sulfonyl) (Rh-PE) lipid was used as the long-chain lipid component. The bicelle samples were hydrated in Tris buffer (10 mM Tris, 150 mM NaCl, pH 7.5) for the quartz crystal microbalance-dissipation (QCM-D) and fluorescence microscopy experiments and in phosphate-buffered saline (PBS; pH 7.4) for cryogenic transmission electron microscopy (cryo-TEM) and antibacterial testing experiments.

2.2. Quartz crystal microbalance-dissipation (QCM-D)

The adsorption, fusogenic, and membrane-disruptive properties of lipid bicelles were characterized by measuring real-time bicelle adsorption onto bare- or supported lipid bilayer-coated silica sensor chip surfaces. The experiments were conducted using a Q-Sense E4 instrument (Biolin Scientific AB, Stockholm, Sweden), as previously described [39-41]. All liquid samples were introduced under continuous flow conditions *via* a peristaltic pump (Reglo Digital MS-4/6, Ismatec, Wertheim, Germany) and the flow rate was fixed at 50 µL/min.

2.3. Time-lapse fluorescence microscopy

Imaging experiments were conducted using a Nikon Eclipse Ti-E inverted microscope that was equipped with a 60× oil-immersion objective lens (NA 1.49), as previously described [39-41]. The adsorption, fusogenic, and membrane-disruptive properties of lipid bicelles were characterized by measuring real-time bicelle adsorption onto glass coverslips enclosed within

a microfluidic chamber (sticky-Slide VI 0.4, ibidi GmbH, Martinsried, Germany). All liquid samples were introduced under continuous flow conditions *via* a peristaltic pump (Reglo Digital MS-4/6, Ismatec, Wertheim, Germany) and the flow rate was fixed at 50 μL/min. Image analysis was conducted using the ImageJ software program (National Institutes of Health, Bethesda, MD, USA).

2.4. Cryogenic transmission electron microscopy (Cryo-TEM)

Bicelle samples were vitrified using a Vitrobot Mark IV (Thermo Fisher, Waltham, MA). Briefly, a 4 μL volume of a bicelle sample was placed on a holey carbon film on a copper grid (Quantioil R2/2, Jena Bioscience GmbH, Jena, Germany). The cryogrid was blotted with filter paper for 2 s and then the film was frozen in liquid ethane (-196 °C). The frozen grid was stored in liquid nitrogen until examination. The experiments were conducted using a Tecnai Arctica transmission electron microscope (Thermo Fisher, Waltham, MA) at 200 kV under low-dose imaging conditions.

2.5. Antibacterial testing

Staphylococcus aureus bacterial cells (ATCC 25923, American Type Culture Collection, Manassas, VA) were prepared at a concentration of 5 x 10^5 colony-forming units (CFU) per mL in PBS and were treated with bicelle samples in a two-fold dilution series for 3 h at 37 °C. The treated bacterial suspensions were subsequently diluted in a 10-fold series, streaked onto Mueller-Hinton agar plates, and the plates were incubated overnight at 37 °C. The minimum bactericidal concentration (MBC) was defined as the minimum bicelle concentration at which the number of viable bacterial cells was reduced by at least 99.99%. Alternatively, the minimum inhibitory concentration (MIC) was determined in applicable cases. All experiments were performed in triplicate.

2.6. Bacterial cell viability testing

The concentration-dependent effect of bicelle samples on *S. aureus* bacterial cell viability was evaluated by using the Live/Dead BacLight Bacterial Viability Kit (Molecular Probes, Invitrogen, Carlsbad, CA). The bacterial cells were prepared at a concentration of 1 x 10^7 CFU/mL in PBS and were treated with bicelle samples in a two-fold dilution series for 3 h at 37 °C. The treated bacterial cells were then stained with the kit dyes so that live and dead bacteria were visualized by green and red colors, respectively. The bacterial cell imaging was performed with a LSM 710 confocal laser scanning microscope (Zeiss, Oberkochen, Germany).

2.7. Statistical analysis

Statistical tests were conducted using the GraphPad Prism software program (San Diego, CA). One-way analysis of variance (ANOVA) with Dunnett's multiple comparisons test was used to evaluate the level of bacterial cell inhibition for different bicelle treatment conditions vs. the bacteria-only control. A multiplicity-adjusted P value of less than 0.05 was the cutoff for statistical significance and *,**,*** indicate $P<0.05$, $P<0.01$, and $P<0.001$, respectively.

3. Results and discussion

3.1. Evaluation of bicelle adsorption and fusogenic properties

We initially characterized DOPC/GML bicelle samples prepared at q-ratio values of 0.05, 0.25, and 2.5 by tracking bicelle adsorption kinetics onto silica-coated surfaces by QCM-D measurements (**Fig. 2**) [39,40]. The QCM-D technique measures the changes in the resonance frequency (Δf) and energy dissipation (ΔD) signals that occur due to bicelle adsorption and are related to the mass and viscoelastic properties of the adsorbed bicelles [54]. Initial measurement baselines in aqueous solution were first recorded before bicelles were added in order to track the measurement responses and the corresponding adsorption kinetics provide insight into the structural properties of the bicelle samples. Depending on the bicelle properties, adsorbing bicelles can either remain intact or fuse to form a supported lipid bilayer (SLB) on the silica surface. SLB formation occurs *via* the fusion and spontaneous rupture of adsorbed bicelles and hence can indicate fusogenic activity, which was signified by final Δf and ΔD shifts around -25 Hz and $< 1 \times 10^{-6}$, respectively [54]. The measurement data are reported for bicelles at each q-ratio and the reported concentrations in this section refer to the DOPC lipid concentration in the bicelles.

q = 0.05

Fig. 2A presents the adsorption kinetics for bicelle adsorption at q = 0.05, in which case the bicelles had a 20-fold greater amount of GML than DOPC. At 0.5-0.031 mM DOPC, two-step adsorption kinetics indicative of bicelle adsorption and fusion-induced spontaneous rupture [34] were observed. At 0.016 mM DOPC, similar adsorption kinetics occurred, however, there was nearly negligible bicelle rupture. The corresponding final Δf and ΔD shifts are presented in **Fig. 2B**. At 0.5 mM DOPC, the final Δf and ΔD shifts were around -26.5 ± 2.8 Hz and 3.8 ± 1.0 × 10^{-6}, respectively. Similar results were obtained at 0.25-0.031 mM DOPC and the final Δf shifts were around -23 to -25 Hz while the final ΔD shifts were around 1.8 to 3.1 × 10^{-6}. The final Δf shifts are consistent with SLB formation, however, the final ΔD shifts are higher than typical SLB values, which suggests the presence of some unruptured bicelles or non-lamellar phase properties within the lipid adlayer [39,40]. For the 0.016 mM DOPC case, the final Δf and ΔD shifts were around -50.6 ± 2.8 Hz and 16.9 ± 0.8 × 10^{-6}, respectively, which likely correspond to a layer of unruptured bicelles. Together, these data support that DOPC/GML bicelles at q = 0.05 can adsorb onto silica surfaces and exhibit fusogenic properties while the results further suggest that the resulting lipid adlayer may exhibit non-lamellar phase properties due to the high concentration of GML in the system.

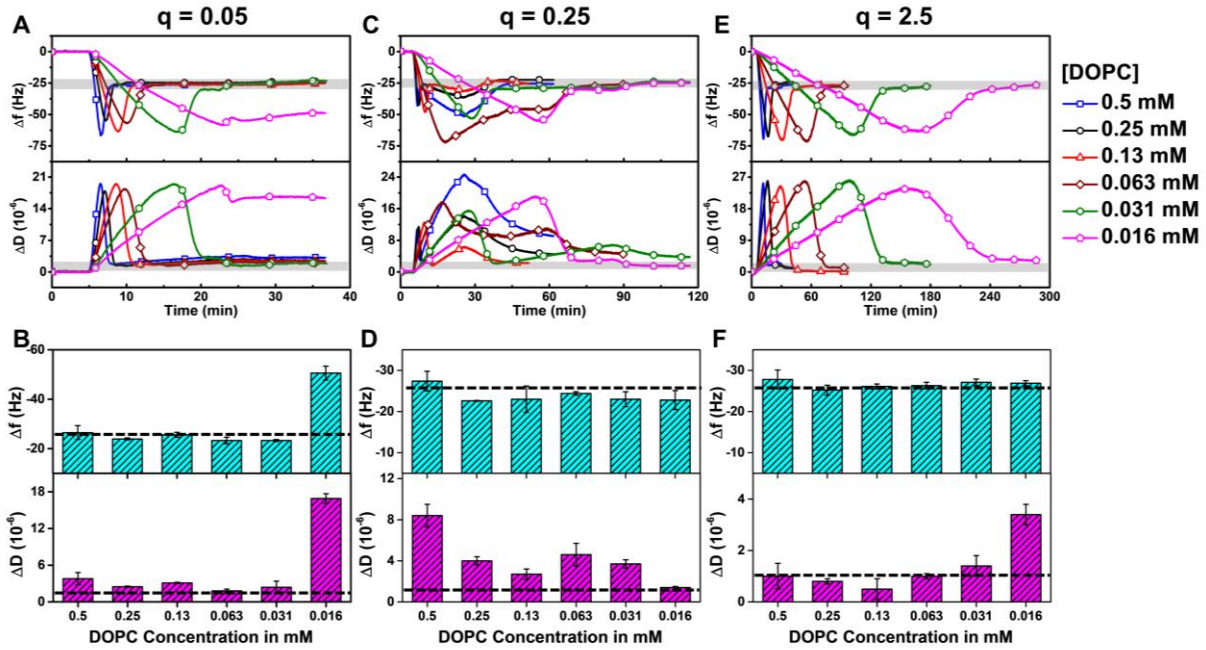

Fig. 2. QCM-D evaluation of DOPC/GML bicelle adsorption and fusogenic activity. (A) QCM-D Δf shifts (upper panel) and ΔD shifts (lower panel) are reported as functions of time for DOPC/GML bicelle adsorption onto silica surfaces for bicelles prepared at q = 0.05. The shaded area in each panel represents the typical measurement responses for bicelle rupture-induced SLB formation. (B) Column graph of the final Δf shifts (upper panel) and ΔD shifts (lower panel) corresponding to the data in panel (A). Data are reported as mean ± s.d. from *n* = 3 measurements. Corresponding QCM-D data and summary values are reported for bicelles prepared at (C-D) q = 0.25 and (E-F) q = 2.5.

q = 0.25

Fig. 2C presents the adsorption kinetics for bicelle adsorption at q = 0.25, in which case the bicelles had a 4-fold greater amount of GML than DOPC. At all tested concentrations, the general adsorption profile showed two steps corresponding to bicelle adsorption and spontaneous rupture. However, closer examination of the adsorption kinetics revealed more complex interaction behavior. At higher concentrations, the typical QCM-D measurement responses associated with bicelle adsorption and rupture leading to SLB formation were followed by decreasing Δf and increasing ΔD shifts afterwards. Such responses likely arise from the membrane-disruptive effects of GML (ref. [50]) and similar effects have been reported for other bicellar systems used for SLB fabrication. On the other hand, GML-induced membrane disruption was less pronounced at lower lipid concentrations, likely due to the lower bulk GML concentration in those cases.

The corresponding final Δf and ΔD shifts are presented in **Fig. 2D**. At 0.5 mM DOPC concentration, the final Δf and ΔD shifts were around -27.4 ± 2.4 Hz and 8.4 ± 1.1 × 10^{-6}, respectively, which point to incomplete SLB formation and the presence of unruptured bicelles and/or GML-induced membrane disruption [39,40]. At lower concentrations, the final Δf and ΔD shifts were in the range of approximately -23 to -25 Hz and 1.5 to 4.5 × 10^{-6}, respectively, which again indicate incomplete SLB formation. Interestingly, the membrane-disruptive effects manifested in the adsorption kinetics were more prominent for DOPC/GML bicelles at q = 0.25 than at q = 0.05 despite lower bulk GML concentrations in the q = 0.25 case, suggesting possible differences in the resulting lipid adlayer properties as well.

q = 2.5

Fig. 2E presents the adsorption kinetics for bicelle adsorption at q = 2.5, in which case the bicelles had a 2.5-fold greater amount of DOPC than GML. At all tested concentrations, there were two-step adsorption kinetics, which indicated fusogenic activity and resulted in SLB formation. The time scale to reach the critical surface coverage of adsorbed bicelles was also inversely proportional to the bulk lipid concentration in line with the diffusion-limited adsorption regime. Notably, at lower lipid concentrations, it took several hours for the rupture process to finish, which is appreciably longer than observed for other bicellar systems. The corresponding final Δf and ΔD shifts are presented in **Fig. 2F** and the final Δf shifts were around -25 to -29 Hz across all tested lipid concentrations, which are within the expected range for SLB adlayers. On the other hand, the corresponding ΔD shifts tended to be higher than normal, with values around 0.5 to 1.5×10^{-6} for 0.5-0.031 mM DOPC lipid concentrations and around 3.5×10^{-6} for 0.016 mM DOPC.

3.2. Morphological characterization of adsorbed bicelle layers

To complement the QCM-D experiments, we also performed time-lapse fluorescence microscopy to track bicelle adsorption and fusogenic activity (**Fig. 3**). The long-chain DOPC lipid population was doped with a fluorescently labeled analogue in order to characterize the morphological properties of adsorbed bicelle layers. Time-lapsed micrographs were captured as bicelles were injected into a microfluidic chamber under continuous flow conditions. The time point at which bicelle adsorption commenced within the microfluidic chamber was defined as t = 0 min. The results for bicelles prepared at each q-ratio and representative lipid concentrations are described below.

q = 0.05

For bicelle adsorption at 0.031 mM DOPC lipid concentration, the fluorescence intensity increased as bicelles adsorbed and a critical surface coverage of adsorbed bicelles was reached after around 9.5 min (**Fig. 3A**). Over time, some dark patches also appeared and the boundaries of these patches kept expanding, which was indicative of bicelle fusion and SLB propagation. After the patches stopped expanding at around 19.5 min, a buffer washing step was performed and the resulting adlayer had two phases consisting of fluorophore-rich and fluorophore-poor regions. This phase separation is reminiscent of how GML can affect lipid dynamics in cellular membranes [55,56]. Furthermore, at 0.016 mM DOPC lipid concentration, the critical surface coverage of adsorbed bicelles was again reached after around 9.4 min and showed two phase-separated regions (**Fig. 3B**). There was nearly negligible evidence of bicelle fusion or SLB propagation, and a buffer wash was performed after the fluorescence intensity stabilized at around 15.8 min. The post-washing appearance of dark spots within the bright phase of the adlayer is likely due to the presence of GML-induced adlayer defects. Hence, the DOPC/GML bicelles prepared at q = 0.05 appear to form phase-separated lipid adlayers.

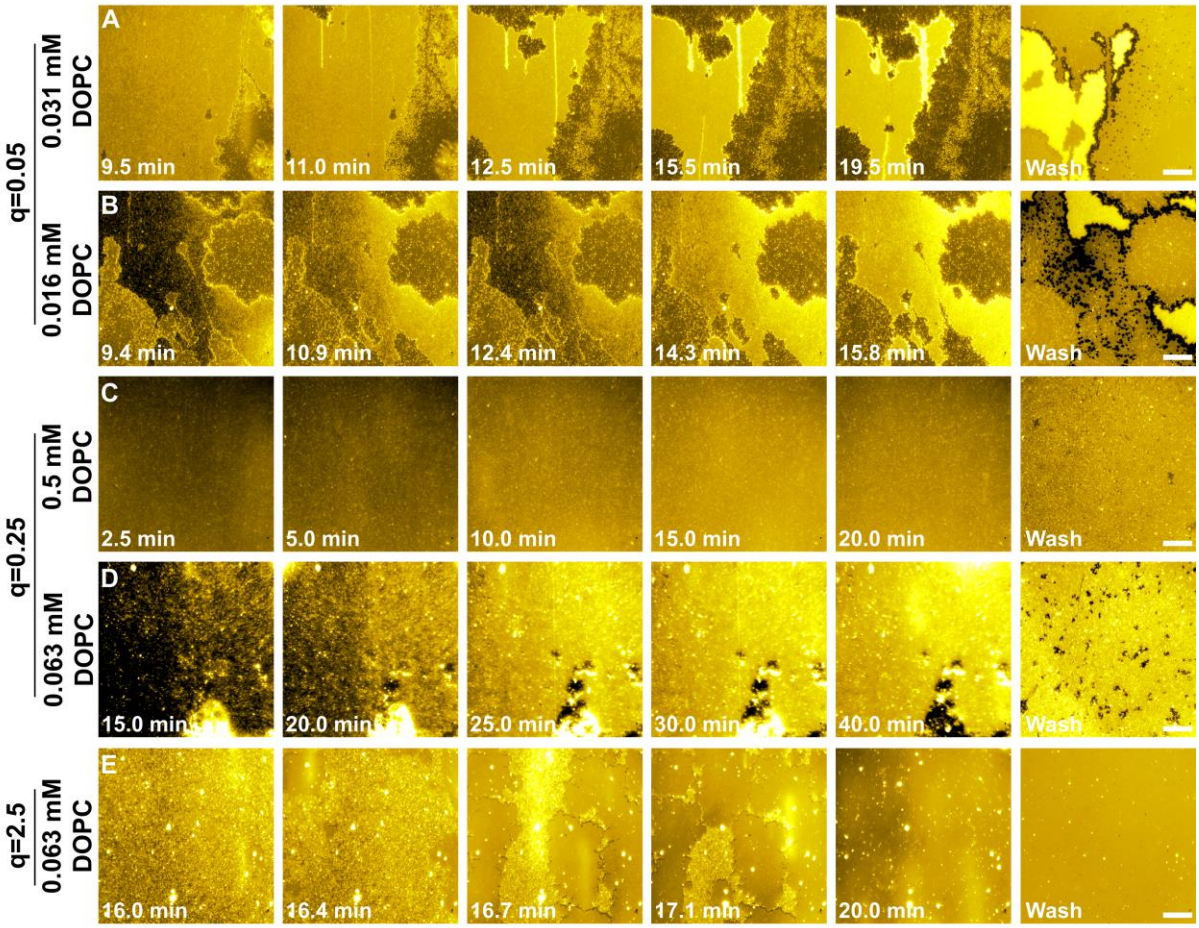

Fig. 3. Time-lapse fluorescence micrographs of lipid adlayers resulting from DOPC/GML bicelle adsorption. Bicelles were added onto a glass surface starting from t = 0 min and the adsorption process was tracked continually until a washing step was performed. The experiments were performed using DOPC/GML bicelles prepared at (A) q = 0.05 and 0.031 mM DOPC, (B) q = 0.05 and 0.016 mM DOPC, (C) q = 0.25 and 0.5 mM DOPC, (D) q = 0.25 and 0.063 mM DOPC, and (E) q = 2.5 and 0.063 mM DOPC. All scale bars are 20 μm.

q = 0.25

For bicelle adsorption at 0.5 mM DOPC lipid concentration, there was a gradual increase in the fluorescence intensity, which indicated continual bicelle adsorption (**Fig. 3C**). Notably, bicelle fusion did not occur and it appeared that a single-phase, adsorbed bicelle layer formed without evidence of SLB formation. Upon a buffer washing step, a small number of dark spots with typical sizes around 2.1 ± 0.1 μm^2 and a total surface area coverage of ~3% also became visible, which indicated GML-induced membrane defects. In line with these observations, for bicelles at 0.063 mM DOPC lipid concentration, the adsorption process was appreciably slower and the fluorescence intensity within the adlayer began to stabilize after around 40 min (**Fig. 3D**). A buffer wash was then performed and the resulting adlayer contained a large number of dark spots, which resembled pore-like defects and had typical sizes around 3.4 ± 0.4 μm^2 that corresponded to a total surface area coverage of ~8%. Together, these findings support that the DOPC/GML bicelles prepared at q = 0.25 can induce pore-like defects within lipid adlayers.

q = 2.5

For this bicelle condition, the QCM-D data indicated that bicelle fusion and SLB formation occurred at all tested lipid concentrations. Accordingly, for bicelle adsorption at 0.063 mM

DOPC lipid concentration, the fluorescence micrographs indicated that a critical surface coverage of adsorbed bicelles was reached after around 16 min, followed by bicelle fusion and SLB propagation (**Fig. 3E**). A nearly complete SLB was formed after around 20 min in total and, upon a buffer washing step, the resulting lipid adlayer exhibited nearly uniform fluorescence intensity with the total surface area coverage of defects corresponding to less than 0.3%, which is indicative of a complete SLB. Hence, DOPC/GML bicelles prepared at q = 2.5 resulted in the formation of a homogenous lipid adlayer consisting of an SLB.

3.3. Evaluation of membrane-disruptive activity

The aforementioned results identified that DOPC/GML bicelles not only exhibit distinct adsorption properties depending on the molar ratio of the DOPC and GML components but also appear to cause membrane-disruptive effects to varying extents. This finding led us to further investigate the membrane-disruptive properties of DOPC/GML bicelles, which expands on past reports that bicelles are useful as nanostructured carriers to incorporate antimicrobial compounds such as membrane-active peptides and antibiotics [57-62]. In this experimental series, we investigated the interactions of DOPC/GML bicelles at different q-ratios with pre-fabricated DOPC SLBs and also tested free GML (defined as q = 0) in parallel (**Fig. 4**). Since GML is the membrane-disruptive component, the GML concentration was fixed at 0.125 mM, at which concentration free GML self-assembles into micelles and has been shown to disrupt SLBs and cause membrane budding [50].

For each experiment, a DOPC SLB was fabricated on a silica surface and then the QCM-D responses were normalized to zero, before the appropriate DOPC/GML bicelle sample or free GML control was added at t = 5 min. The corresponding QCM-D measurement responses are presented in **Fig. 4A** and showed that the DOPC/GML bicelles interact with the DOPC SLB. In general, modest decreases in the Δf signal were accompanied by larger increases in the ΔD signal, which indicated membrane morphological changes reminiscent of membrane budding [47] due to bicelle addition. A buffer washing step was then performed and the measurement responses partially recovered while there were still pronounced changes in membrane morphology post-washing. Overall, the initial QCM-D measurement responses were appreciably smaller than that of free GML tested at the same concentration (see insets in Fig. 4A), which indicates that the bicellar nanostructure design can modulate the degree of membrane-disruptive activity. Notably, however, the post-washing ΔD shifts were larger for the lipid adlayers treated with the DOPC/GML bicelles as opposed to free GML, indicating more permanent membrane damage.

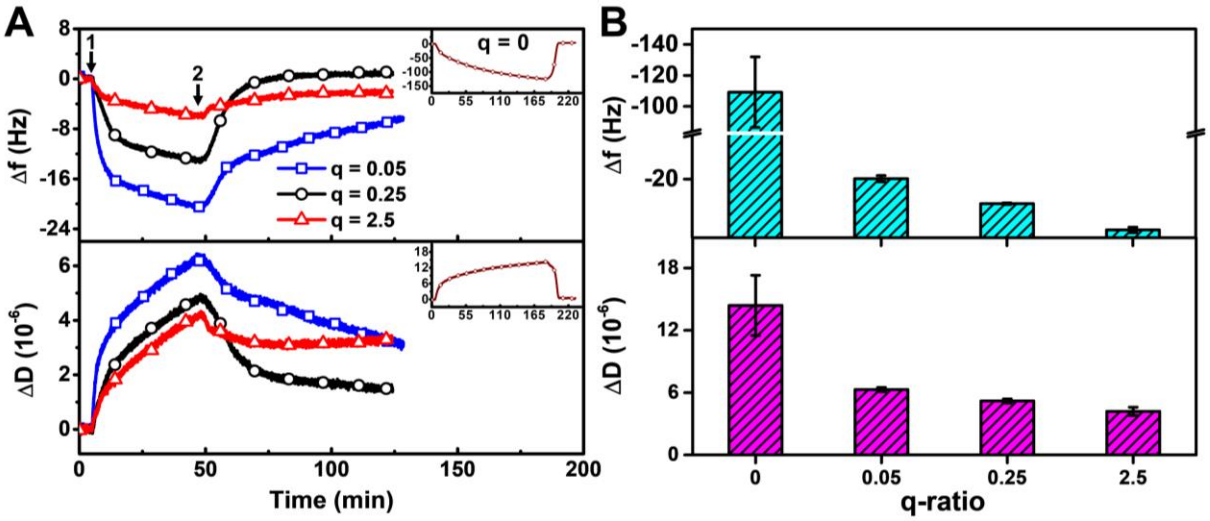

Fig. 4. QCM-D tracking of DOPC/GML bicelle interactions with DOPC SLBs. (A) QCM-D Δf shifts (upper panel) and ΔD shifts (lower panel) due to DOPC/GML bicelle interactions with DOPC SLBs are reported as functions of time. The initial baseline values correspond to a prefabricated DOPC SLB and then DOPC/GML bicelles at different q-ratios were added at around t = 5 min (see arrow 1) followed by a buffer washing step (see arrow 2). The GML concentration was fixed at 0.125 mM in all experiments. Insets show corresponding data for free GML (equivalent to q = 0). (B) Column graph of the final Δf shifts (upper panel) and ΔD shifts (lower panel) corresponding to the data in panel (A). Data are reported as mean ± s.d. from n = 3 measurements.

Fig. 4B summarizes the maximum Δf and ΔD shifts that occurred due to the SLB interaction with DOPC/GML bicelles or free GML. For DOPC/GML bicelles prepared at q = 0.05, the maximum Δf and ΔD shifts were around -20.1 ± 0.8 Hz and 6.3 ± 0.2 × 10^{-6}, respectively. Similar levels of membrane-disruptive activity were observed for DOPC/GML bicelles prepared at q = 0.25, in which case the maximum Δf and ΔD shifts were around -13.7 ± 0.2 Hz and 5.2 ± 0.2 × 10^{-6}, respectively. On the other hand, for DOPC/GML bicelles prepared at q = 2.5, the maximum Δf and ΔD shifts were much smaller and around -7.0 ± 0.7 Hz and 4.2 ± 0.4 × 10^{-6}, respectively. By contrast, the addition of free GML led to maximum Δf and ΔD shifts of around -109.2 ± 22.8 Hz and 14.4 ± 2.9 × 10^{-6}, respectively.

Taken together, the results show that bicelles prepared at q = 0.05 have appreciable membrane-disruptive activity, moderate activity at q = 0.25, and minor activity at q = 2.5 when compared to the significantly greater activity of free GML alone. This trend further supports that the DOPC component within bicelles modulates the extent of membrane-disruptive activity of GML depending on the molar ratio of the two bicelle components. Based on these results, we selected DOPC/GML bicelles prepared at q = 0.25 as the lead bicelle composition for antibacterial activity testing due to (1) a relatively high degree of membrane-disruptive activity and (2) evidence of pore-like membrane disruption, which could be useful for inhibiting bacterial cell membranes. By contrast, DOPC/GML bicelles prepared at q = 0.05 induced membrane phase separation but not pore-like membrane disruption, while the DOPC/GML bicelles prepared at q = 2.5 had a relatively low degree of membrane-disruptive activity.

3.4. Antibacterial activity testing

We initially conducted cryogenic transmission electron microscopy (cryo-TEM) experiments to characterize the structural morphology of the DOPC/GML bicelles prepared at q = 0.25, which were used in the antibacterial testing experiments. As presented in **Fig. 5A**, spherical, lamellar-phase structures were observed in the cryo-TEM micrographs and the typical size distribution was around 100 to 600 nm. The lamellar-phase vesicular organization was consistent with other bicellar nanostructures described in the literature [63] and additional dynamic light scattering experiments showed that the mean diameter of the DOCP/GML bicelles was around 479 ± 116 nm. Altogether, these data support that the DOPC/GML bicelles prepared at q = 0.25 had a nanostructured architecture, lamellar-phase properties, and fusogenic activity as described above.

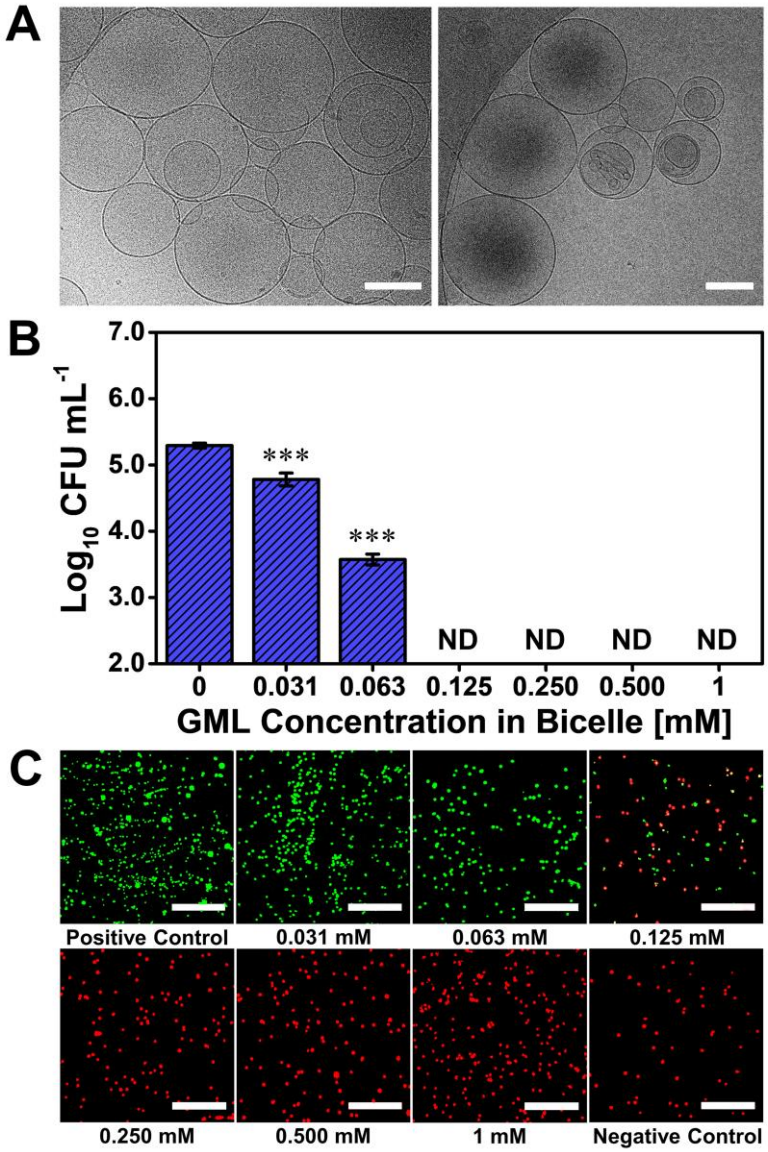

Fig. 5. Antibacterial testing of DOPC/GML bicelles to inhibit *S. aureus* bacteria. (A) Cryo-TEM micrographs of DOPC/GML bicelles prepared at q = 0.25. All scale bars are 200 nm. (B) Effect of DOPC/GML bicelle (q = 0.25) treatment on the number concentration of *S. aureus* bacterial cells. The bicelle amount was defined based on the corresponding GML concentration. Data are expressed in CFU/mL units and ND means that no viable bacterial cells were detected. Mean ± standard deviation are reported from *n* = 3 experiments. (C) Effect of DOPC/GML bicelle (q = 0.25) treatment on *S. aureus* bacterial cell viability by confocal laser scanning microscopy (CLSM) imaging. The bicelle amount was defined based on the corresponding GML concentration. Live and dead bacterial cells are represented by green and red colors, respectively. Representative images are presented from triplicate experiments and all scale bars are 50 μm.

We proceeded to evaluate the concentration-dependent effect of DOPC/GML bicelles on *S. aureus* bacterial cell viability based on a colony-forming unit (CFU) enumeration assay (**Fig. 5B**). An initial inoculum of 5 x 10^5 CFU/mL bacterial cells was incubated with different amounts of DOPC/GML bicelles for 3 h and the resulting degree of cell viability was then measured based on colony growth. The data are reported in terms of the effective GML concentration that was present within the DOPC/GML bicelles. Treatment with 0.031 mM GML caused the *S. aureus* cell viability to decrease to around 8×10^4 CFU/mL, while treatment

with 0.063 mM GML caused a further drop to around 4×10^3 CFU/mL. At 0.125 mM and higher GML concentrations, the *S. aureus* cell viability had dropped to undetectable levels and hence the minimum bactericidal concentration (MBC) for DOPC/GML bicelles prepared at q = 0.25 was determined to be 0.125 mM GML.

Confocal laser scanning microscopy experiments were also performed to directly visualize the effects of DOPC/GML bicelle treatment on *S. aureus* cell viability (**Fig. 5C**). An initial inoculum of 1 x 10^7 CFU/mL bacterial cells was incubated with different amounts of DOPC/GML bicelles for 3 h and the resulting degree of cell viability was then measured by dye staining and microscopic observation. Live cells were visualized by the SYTO 9 dye (green color) while dead cells were visualized by the PI dye (red color), which could only translocate through the membranes of dead bacterial cells [64]. Up to 0.063 mM GML, most cells remained alive while a marked transition occurred around 0.125 mM GML, at which condition there were large fractions of live and dead cells. At 0.25 mM and higher GML concentrations, all cells appeared dead and these results provided confirmatory evidence that DOPC/GML bicelles prepared at q = 0.25 can kill *S. aureus* bacterial cells. In combination with the biophysical data, the experimentally observed bactericidal activity of DOPC/GML bicelles is consistent with the known membrane-disruptive properties of GML against Gram-positive bacteria while additional mechanisms of antibacterial activity beyond bacterial cell membrane disruption alone are also possible.

Additional growth inhibition experiments with 5×10^5 CFU/mL *S. aureus* bacterial cells showed that the minimum inhibitory concentration (MIC) value for DOPC/GML bicelles prepared at q = 0.25 was also 0.125 mM GML while no MIC was determined for DOPC/GML bicelles prepared at q = 2 due to lack of effective antibacterial activity for that sample. Moreover, no MIC values were determined for DOPC/DHPC bicelles prepared at q = 0.25 and q = 2, which were tested in parallel and contained DHPC – a short-chain, detergent-like phospholipid that is commonly used for bicelle preparation – in lieu of GML. Together, these findings demonstrate that the specific design parameters of the DOPC/GML bicelles are important for conferring antibacterial activity, including the presence of GML as the active functional component and the q-ratio that influences both the DOPC/GML molar ratio and nanostructured bicelle morphology.

4. Conclusions and outlook

In this study, we have demonstrated that DOPC/GML bicelles can exhibit a wide range of membrane-disruptive properties and inhibit *S. aureus* bacteria based on a killing mechanism. While bicelles have long been utilized as passive structural carriers to host other classes of biologically active molecules such as antibiotics and antimicrobial peptides, our findings demonstrate that the molecular components used to fabricate bicelles can be rationally tuned to endow bicelles with active functional properties such as antibacterial activity. Importantly, not all types of bicelles demonstrate antibacterial activity or membrane-disruptive behavior and there are key bicelle design parameters such as the lipid composition and q-ratio. While free GML has been reported to exhibit antibacterial and antiviral activity, GML is mainly active in the micellar form above a critical bulk concentration and is hence sensitive to dilutions that can limit application utility. By contrast, the results in this study demonstrate that DOPC/GML bicelles self-assemble into lamellar-phase nanostructures with vesicular organization, which can enhance structural stability and overcome dilution challenges associated with micellar assemblies. Furthermore, the aqueous cavity and/or the lipid bilayer shell of the fabricated DOPC/GML bicelles can also be loaded with other functional components to enhance

application possibilities. Together, these findings demonstrate how lipid bicelle engineering can help to shift the paradigm from bicelles as passive carriers to bicelles as biologically active nanostructures with important functional properties such as antibacterial activity.

Acknowledgments

This work was supported by the National Research Foundation of Singapore through a Proof-of-Concept grant (NRF2015NRF-POC0001-19), and by the National Research Foundation of Korea (NRF) grant funded by the Korean government (MSIT) (2020R1C1C1004385). In addition, this work was supported by the Korea Research Fellowship Program through the National Research Foundation of Korea (NRF) funded by the Ministry of Science and ICT (2019H1D3A1A01070318). This research was also supported by the International Research & Development Program of the National Research Foundation of Korea (NRF) funded by the Ministry of Science and ICT (2020K1A3A1A39112724).

Data availability

The raw data required to reproduce these findings are available from the corresponding authors on reasonable request.

References

[1] Marcotte, I., and Auger, M., Bicelles as model membranes for solid-and solution-state NMR studies of membrane peptides and proteins, Concepts Magn. Reson., Part A 1 (2005) 17-37.
[2] Hu, A., Fan, T.-H., Katsaras, J., Xia, Y., Li, M., Nieh, M.-P., Lipid-based nanodiscs as models for studying mesoscale coalescence–a transport limited case, Soft Matter 28 (2014) 5055-5060.
[3] Caldwell, T. A., Baoukina, S., Brock, A. T., Oliver, R. C., Root, K. T., Krueger, J. K., Glover, K. J., Tieleman, D. P., Columbus, L., Low-*q* bicelles are mixed micelles, J. Phys. Chem. Lett. 15 (2018) 4469-4473.
[4] Dürr, U. H., Soong, R., Ramamoorthy, A., When detergent meets bilayer: birth and coming of age of lipid bicelles, Prog. Nucl. Magn. Reson. Spectrosc. (2013) 1-22.
[5] Nieh, M.-P., Raghunathan, V., Glinka, C. J., Harroun, T. A., Pabst, G., Katsaras, J., Magnetically alignable phase of phospholipid "bicelle" mixtures is a chiral nematic made up of wormlike micelles, Langmuir 19 (2004) 7893-7897.
[6] Katsaras, J., Harroun, T. A., Pencer, J., Nieh, M.-P., "Bicellar" lipid mixtures as used in biochemical and biophysical studies, Naturwissenschaften 8 (2005) 355-366.
[7] Harroun, T. A., Koslowsky, M., Nieh, M.-P., de Lannoy, C.-F., Raghunathan, V., Katsaras, J., Comprehensive examination of mesophases formed by DMPC and DHPC mixtures, Langmuir 12 (2005) 5356-5361.
[8] van Dam, L., Karlsson, G., Edwards, K., Morphology of magnetically aligning DMPC/DHPC aggregates perforated sheets, not disks, Langmuir 7 (2006) 3280-3285.
[9] Pabst, G., Kučerka, N., Nieh, M.-P., Rheinstädter, M., Katsaras, J., Applications of neutron and X-ray scattering to the study of biologically relevant model membranes, Chem. Phys. Lipids 6 (2010) 460-479.
[10] Nieh, M.-P., Raghunathan, V., Pabst, G., Harroun, T., Nagashima, K., Morales, H., Katsaras, J., Macdonald, P., Temperature driven annealing of perforations in bicellar model membranes, Langmuir 8 (2011) 4838-4847.

[11] Li, M., Morales, H. H., Katsaras, J., Kučerka, N., Yang, Y., Macdonald, P. M., Nieh, M.-P., Morphological characterization of DMPC/CHAPSO bicellar mixtures: a combined SANS and NMR study, Langmuir 51 (2013) 15943-15957.
[12] Ariga, K., Leong, D. T., Mori, T., Nanoarchitectonics for Hybrid and Related Materials for Bio-Oriented Applications, Adv. Funct. Mater. 27 (2018) 1702905.
[13] Ariga, K., Mori, T., Li, J., Langmuir nanoarchitectonics from basic to frontier, Langmuir 10 (2018) 3585-3599.
[14] Vold, R. R., Prosser, R. S., Deese, A. J., Isotropic solutions of phospholipid bicelles: a new membrane mimetic for high-resolution NMR studies of polypeptides, J. Biomol. NMR 3 (1997) 329-335.
[15] van Dam, L., Karlsson, G., Edwards, K., Direct observation and characterization of DMPC/DHPC aggregates under conditions relevant for biological solution NMR, Biochim. Biophys. Acta, Biomembr. 2 (2004) 241-256.
[16] De Angelis, A. A., and Opella, S. J., Bicelle samples for solid-state NMR of membrane proteins, Nat. Protoc. 10 (2007) 2332.
[17] Lin, L., Wang, X., Guo, Y., Ren, K., Li, X., Jing, L., Yue, X., Zhang, Q., Dai, Z., Hybrid bicelles as a pH-sensitive nanocarrier for hydrophobic drug delivery, RSC Adv. 83 (2016) 79811-79821.
[18] Lin, L., Liang, X., Xu, Y., Yang, Y., Li, X., Dai, Z., Doxorubicin and indocyanine green loaded hybrid bicelles for fluorescence imaging guided synergetic chemo/photothermal therapy, Bioconjugate Chem. 9 (2017) 2410-2419.
[19] Uchida, N., Nishizawa Horimoto, N., Yamada, K., Hikima, T., Ishida, Y., Kinetically stable bicelles with dilution tolerance, size tunability, and thermoresponsiveness for drug delivery applications, ChemBioChem 18 (2018) 1922-1926.
[20] Barbosa-Barros, L., Barba, C., Cócera, M., Coderch, L., López-Iglesias, C., de La Maza, A., López, O., Effect of bicellar systems on skin properties, Int. J. Pharm. 1-2 (2008) 263-272.
[21] Barbosa-Barros, L., de La Maza, A., Estelrich, J., Linares, A., Feliz, M., Walther, P., Pons, R., López, O., Penetration and growth of DPPC/DHPC bicelles inside the stratum corneum of the skin, Langmuir 11 (2008) 5700-5706.
[22] Rodriguez, G., Barbosa-Barros, L., Rubio, L., Cócera, M., Díez, A., Estelrich, J., Pons, R., Caelles, J., Maza, A. D. l., López, O., Conformational changes in stratum corneum lipids by effect of bicellar systems, Langmuir 18 (2009) 10595-10603.
[23] Rubio, L., Alonso, C., Rodríguez, G., Barbosa-Barros, L., Coderch, L., De la Maza, A., Parra, J., Lopez, O., Bicellar systems for in vitro percutaneous absorption of diclofenac, Int. J. Pharm. 1-2 (2010) 108-113.
[24] Rodríguez, G., Barbosa-Barros, L., Rubio, L., Cócera, M., López-Iglesias, C., de la Maza, A., López, O., Bicellar systems as modifiers of skin lipid structure, Colloids Surf., B 2 (2011) 390-394.
[25] Rubio, L., Rodríguez, G., Barbosa-Barros, L., Alonso, C., Cócera, M., de la Maza, A., Parra, J., López, O., Bicellar systems as a new colloidal delivery strategy for skin, Colloids Surf., B (2012) 322-326.
[26] Barbosa-Barros, L., Rodríguez, G., Barba, C., Cócera, M., Rubio, L., Estelrich, J., López-Iglesias, C., de la Maza, A., López, O., Bicelles: lipid nanostructured platforms with potential dermal applications, Small 6 (2012) 807-818.
[27] Rubio, L., Alonso, C., Rodríguez, G., Cócera, M., López-Iglesias, C., Coderch, L., De la Maza, A., Parra, J., López, O., Bicellar systems as new delivery strategy for topical application of flufenamic acid, Int. J. Pharm. 1-2 (2013) 60-69.

[28] Rodríguez, G., Barbosa-Barros, L., Rubio, L., Cócera, M., Fernández-Campos, F., Calpena, A., Fernández, E., De La Maza, A., López, O., Bicelles: new lipid nanosystems for dermatological applications, J. Biomed. Nanotechnol. 2 (2015) 282-290.
[29] Zeineldin, R., Last, J. A., Slade, A. L., Ista, L. K., Bisong, P., O'Brien, M. J., Brueck, S., Sasaki, D. Y., Lopez, G. P., Using bicellar mixtures to form supported and suspended lipid bilayers on silicon chips, Langmuir 19 (2006) 8163-8168.
[30] Tabaei, S. R., Jönsson, P., Brändén, M., Höök, F., Self-assembly formation of multiple DNA-tethered lipid bilayers, J. Struct. Biol. 1 (2009) 200-206.
[31] Morigaki, K., Kimura, S., Okada, K., Kawasaki, T., Kawasaki, K., Formation of substrate-supported membranes from mixtures of long-and short-chain phospholipids, Langmuir 25 (2012) 9649-9655.
[32] Saleem, Q., Zhang, Z., Petretic, A., Gradinaru, C. C., Macdonald, P. M., Single lipid bilayer deposition on polymer surfaces using bicelles, Biomacromolecules 3 (2015) 1032-1039.
[33] Yamada, N. L., Sferrazza, M., Fujinami, S., In-situ measurement of phospholipid nanodisk adhesion on a solid substrate using neutron reflectometry and atomic force microscopy, Phys. B: Condens. Matter (2018) 222-226.
[34] Kolahdouzan, K., Jackman, J. A., Yoon, B. K., Kim, M. C., Johal, M. S., Cho, N.-J., Optimizing the formation of supported lipid bilayers from bicellar mixtures, Langmuir 20 (2017) 5052-5064.
[35] Sut, T. N., Jackman, J. A., Cho, N.-J., Understanding how membrane surface charge influences lipid bicelle adsorption onto oxide surfaces, Langmuir 25 (2019) 8436-8444.
[36] Sut, T. N., Jackman, J. A., Yoon, B. K., Park, S., Kolahdouzan, K., Ma, G. J., Zhdanov, V. P., Cho, N.-J., Influence of NaCl concentration on bicelle-mediated SLB formation, Langmuir 32 (2019) 10658-10666.
[37] Sut, T. N., Park, S., Choe, Y., Cho, N.-J., Characterizing the supported lipid membrane formation from cholesterol-rich bicelles, Langmuir 47 (2019) 15063-15070.
[38] Jackman, J. A., and Cho, N.-J., Supported lipid bilayer formation: beyond vesicle fusion, Langmuir 6 (2020) 1387-1400.
[39] Sut, T. N., Park, S., Yoon, B. K., Jackman, J. A., Cho, N.-J., Supported lipid bilayer formation from phospholipid-fatty acid bicellar mixtures, Langmuir 18 (2020) 5021-5029.
[40] Sut, T. N., Park, S., Yoon, B. K., Jackman, J. A., Cho, N.-J., Optimal formation of uniform-phase supported lipid bilayers from phospholipid-monoglyceride bicellar mixtures, J. Ind. Eng. Chem. (2020) 285-291.
[41] Sut, T. N., Yoon, B. K., Park, S., Jackman, J. A., Cho, N.-J., Versatile formation of supported lipid bilayers from bicellar mixtures of phospholipids and capric acid, Sci. Rep. (2020) 13849.
[42] Thakur, A., Sharma, N., Bhatti, M., Sharma, M., Trukhanov, A. V., Trukhanov, S. V., Panina, L. V., Astapovich, K. A., Thakur, P., Synthesis of barium ferrite nanoparticles using rhizome extract of *Acorus calamus*: characterization and its efficacy against different plant phytopathogenic fungi, Nano-Struct. Nano-Objects (2020) 100599.
[43] Jackman, J. A., Lee, J., Cho, N. J., Nanomedicine for infectious disease applications: innovation towards broad-spectrum treatment of viral infections, Small 9 (2016) 1133-1139.
[44] Chen, L., and Liang, J., Materials Science and Engineering: C, Mater. Sci. Eng.: C (2020) 110924.
[45] Abo-Zeid, Y., and Williams, G. R., The potential anti-infective applications of metal oxide nanoparticles: a systematic review, Wiley Interdiscip. Rev.: Nanomed. Nanobiotechnol. 2 (2020) e1592.
[46] Kabara, J. J., Swieczkowski, D. M., Conley, A. J., Truant, J. P., Fatty acids and derivatives as antimicrobial agents, Antimicrob. Agents Chemother. 1 (1972) 23-28.

[47] Conley, A. J., and Kabara, J. J., Antimicrobial action of esters of polyhydric alcohols, Antimicrob. Agents Chemother. 5 (1973) 501-506.
[48] Schlievert, P. M., and Peterson, M. L., Glycerol monolaurate antibacterial activity in broth and biofilm cultures, PloS One 7 (2012) e40350.
[49] Li, Q., Estes, J. D., Schlievert, P. M., Duan, L., Brosnahan, A. J., Southern, P. J., Reilly, C. S., Peterson, M. L., Schultz-Darken, N., Brunner, K. G., Glycerol monolaurate prevents mucosal SIV transmission, Nature 458 (2009) 1034-1038.
[50] Yoon, B. K., Jackman, J. A., Kim, M. C., Cho, N.-J., Spectrum of membrane morphological responses to antibacterial fatty acids and related surfactants, Langmuir 37 (2015) 10223-10232.
[51] Fu, X., Feng, F., Huang, B., Physicochemical characterization and evaluation of a microemulsion system for antimicrobial activity of glycerol monolaurate, Int. J. Pharm. 1-2 (2006) 171-175.
[52] Fu, X., Zhang, M., Huang, B., Liu, J., Hu, H., Feng, F., Enhancement of antimicrobial activities by the food-grade monolaurin microemulsion system, J. Food Process Eng. 1 (2009) 104-111.
[53] Turner, N. A., Sharma-Kuinkel, B. K., Maskarinec, S. A., Eichenberger, E. M., Shah, P. P., Carugati, M., Holland, T. L., Fowler, V. G., Methicillin-resistant Staphylococcus aureus: an overview of basic and clinical research, Nat. Rev. Microbiol. 4 (2019) 203-218.
[54] Cho, N.-J., Frank, C. W., Kasemo, B., Höök, F., Quartz crystal microbalance with dissipation monitoring of supported lipid bilayers on various substrates, Nat. Protoc. 6 (2010) 1096.
[55] Zhang, M. S., Sandouk, A., Houtman, J. C., Glycerol Monolaurate (GML) inhibits human T cell signaling and function by disrupting lipid dynamics, Sci. Rep. (2016) 30225.
[56] Zhang, M. S., Tran, P. M., Wolff, A. J., Tremblay, M. M., Fosdick, M. G., Houtman, J. C., Glycerol monolaurate induces filopodia formation by disrupting the association between LAT and SLP-76 microclusters, Sci. Signal. 528 (2018) eaam9095.
[57] Oliveira, T. R., Benatti, C. R., Lamy, M. T., Structural characterization of the interaction of the polyene antibiotic amphotericin B with DODAB bicelles and vesicles, Biochim. Biophys. Acta, Biomembr. 11 (2011) 2629-2637.
[58] Dittmer, J., Thøgersen, L., Underhaug, J., Bertelsen, K., Vosegaard, T., Pedersen, J. M., Schiøtt, B., Tajkhorshid, E., Skrydstrup, T., Nielsen, N. C., Incorporation of antimicrobial peptides into membranes: a combined liquid-state NMR and molecular dynamics study of alamethicin in DMPC/DHPC bicelles, J. Phys. Chem. B 19 (2009) 6928-6937.
[59] Whiles, J. A., Brasseur, R., Glover, K. J., Melacini, G., Komives, E. A., Vold, R. R., Orientation and effects of mastoparan X on phospholipid bicelles, Biophys. J. 1 (2001) 280-293.
[60] Bortolus, M., Dalzini, A., Toniolo, C., Hahm, K. S., Maniero, A. L., Interaction of hydrophobic and amphipathic antimicrobial peptides with lipid bicelles, J. Pept. Sci. 7 (2014) 517-525.
[61] Raja, Z., André, S., Abbassi, F., Humblot, V., Lequin, O., Bouceba, T., Correia, I., Casale, S., Foulon, T., Sereno, D., Insight into the mechanism of action of temporin-SHa, a new broad-spectrum antiparasitic and antibacterial agent, PloS One 3 (2017) e0174024.
[62] Mamusa, M., Salvatore, A., Berti, D., Structural modifications of DPPC bilayers upon inclusion of an antibacterial cationic bolaamphiphile, Langmuir 30 (2018) 8952-8961.
[63] Rodríguez, G., Cócera, M., Rubio, L., López-Iglesias, C., Pons, R., de la Maza, A., López, O., A unique bicellar nanosystem combining two effects on stratum corneum lipids, Mol. Pharmaceutics 3 (2012) 482-491.

[64] Robertson, J., McGoverin, C., Vanholsbeeck, F., Swift, S., Optimisation of the protocol for the LIVE/DEAD® BacLight™ Bacterial Viability Kit for rapid determination of bacterial load, Front. Microbiol. (2019) 801.